Article

Near Infrared Light Activates Molecular Nanomachines to Drill Into and Kill Cells

Dongdong Liu, Víctor García-López, Richard S. Gunasekera, Lizanne Greer Nilewski, Lawrence B. Alemany, Amir Aliyan, Tao Jin, Gufeng Wang, James M. Tour, and Robert Pal

Just Accepted

Near Infrared Light Activates Molecular Nanomachines to Drill Into and Kill Cells

Dongdong Liu,[†] Víctor García-López,[†] Richard S. Gunasekera,[†,]

[a] Lizanne Greer Nilewski,[†] Lawrence B. Alemany,[†,ʃ] Amir Aliyan,[†] Tao Jin,[ʃ] Gufeng Wang,[ʃ,]*

James M. Tour[†,¥,]* and Robert Pal[ξ,]*

[†]Department of Chemistry, [ʃ]Shared Equipment Authority, [¥]Department of Materials Science and

NanoEngineering, [¥]Smalley-Curl Institute and [¥]NanoCarbon Center, Rice University, Houston,

Texas 77005, United States.

[ʃ]Department of Chemistry, North Carolina State University, Raleigh, NC 27695-8204. United

States. [ξ]Department of Chemistry, Durham University, South Road, DH1 3LE Durham, United

Kingdom

E-Mail: gwang10@ncsu.edu, tour@rice.edu, robert.pal@durham.ac.uk

Abstract

Using two-photon excitation (2PE), molecular nanomachines (MNMs) are able to drill through cell membranes and kill the cells. This avoids the use of the more damaging ultraviolet (UV) light that has been used formerly to induce this nanomechanical cell-killing effect. Since 2PE is inherently confocal, enormous precision can be realized. The MNMs can be targeted to specific cell surfaces through peptide addends. Further, the efficacy was verified through controlled opening of synthetic bilayer vesicles using the 2PE excitation of MNM that had been trapped within the vesicles.

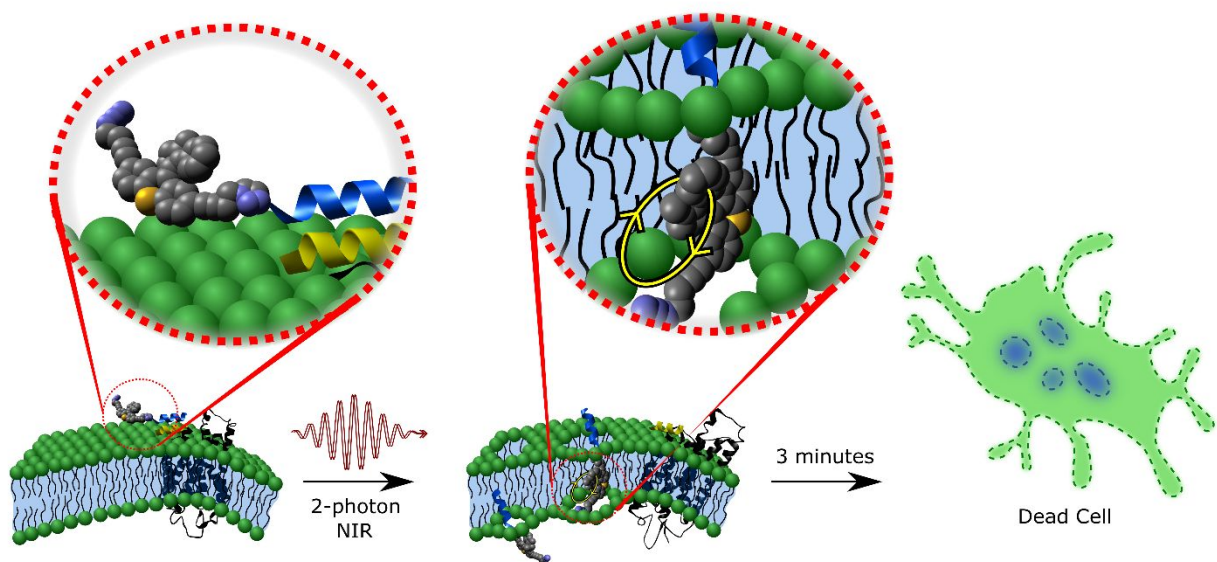[a] Current Address: Biola University, School of Science, Technology and Health, 13800 Biola Ave, La Mirada CA 90639.

Additional modes of efficient cell killing are essential for treatment of several pathologies including cancers and antibiotic-resistant bacteria. Using a specifically designed generation of Feringa-type light-activated cell-specific molecular nanomachines (MNMs), we formerly demonstrated the use of UV-actuated molecular mechanical action to open cellular membranes thereby expediting cell death.[1] In the work here, nanomechanical activation is enabled by using two-photon excitation (2PE) near-infrared (NIR) light, thus using a wavelength of light that is less destructive to cells. This combines peptide-directed cell-specific targeting using MNMs and biologically safer NIR activation. The approach permits single-cell-death optical-precision.[2,3] Thus targeted photodynamic therapy protocols are enabled by target-receptor-specific MNMs resulting in rapid eradication of specific cell types using a biologically safe wavelength of light.

An important need for future global healthcare and more specifically for personalized therapeutics is the effective targeting and destruction of selected cells and cell types, as recently being realized by the emergence of powerful optogenetic strategies.[4] Beyond the more common chemical delivery strategies, several physical techniques are available to target and modulate cellular membranes. These techniques include electric and magnetic fields, temperature, ultrasound and light to introduce compounds into cells, release molecular species from cells, or to selectively induce apoptosis or necrosis.[5-10] With the advent of molecular motors and switches that can change their conformation in response to external stimuli, such as light, an approach for molecular mechanical therapeutics is being enabled.[11]

We formerly showed that by using MNMs with 355-365 nm UV-light activation, and

capitalizing upon their rotor speeds of 2-3 MHz,[12] they drilled through cell membranes.[1] However,

we had concern regarding the inherent UV-induced damage that was simultaneously occurring. In

order to address this secondary UV-induced injury, we use here a more biologically preferred and

less destructive NIR light through 2PE at 710-720 nm in a 3-dimensional (3D) raster pattern. The

inherent 3D precision 2PE is so high that only surface bound MNM-bearing cancer cells undergo

cell death; all neighboring cells remain intact and unaffected in a 3D *in vitro* matrix of cells and

MNMs.

a

2-photon
NIR

3 minutes

Dead Cell

b

Rotor

R

Stator

R, R' = functional addends or H

1
2
3
4
5
6
7
8
9
10
11
12
13
14
15
16
17
18
19
20
21
22
23
24
25
26
27
28
29
30
31
32
33
34
35
36
37
38
39
40
41
42
43
44
45
46
47
48
49
50
51
52
53
54
55
56
57
58
59
60

c

1 (untargeted, fast motor)

2 (untargeted, slow motor, control)

3 (untargeted, no rotor, control)

4 (mono-SNTRVAP, PC3-targeted, fast motor)

5 (mono-DMPGTVLP, MCF7-targeted, fast motor)

6 (fluorescent, fast motor)

4
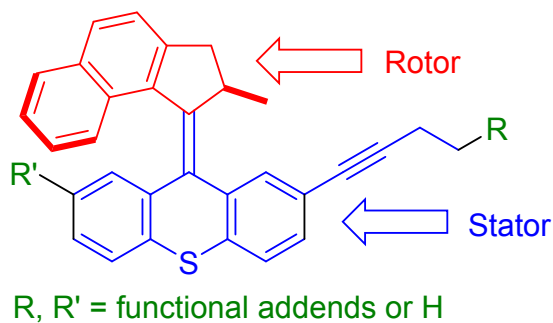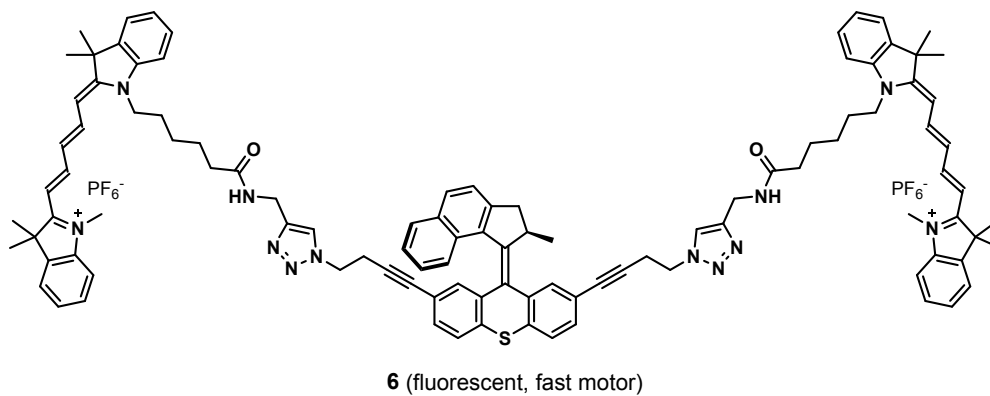
Figure 1. MNMs for 2PE disruption of lipid bilayers through molecular mechanical action along with control molecules. (a) Schematic of a molecular machine selectively binding to the membrane surface through a peptide recognition and then drilling through a cell membrane by NIR 2PE-activated molecular mechanical action to kill the cell (by William K. A. Sikkema). (b) The representative molecular machine shows the rotor portions in red, which is light-activated to rotate unidirectionally relative to the larger bottom blue stator portion; the green addends (R and R') are varied to provide the requisite solubility or recognition sites for cellular targeting. (c) Detailed chem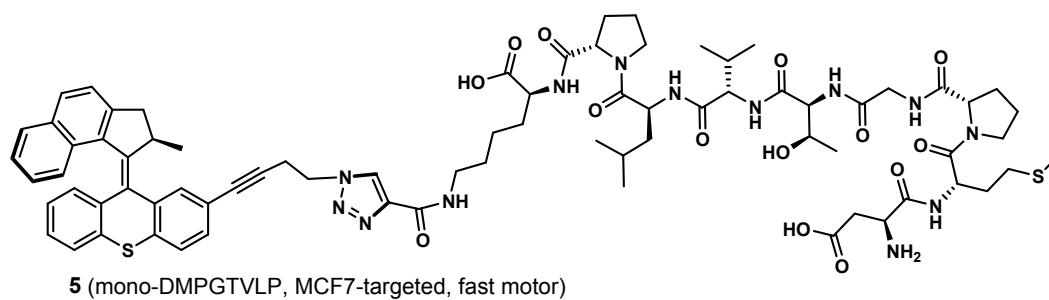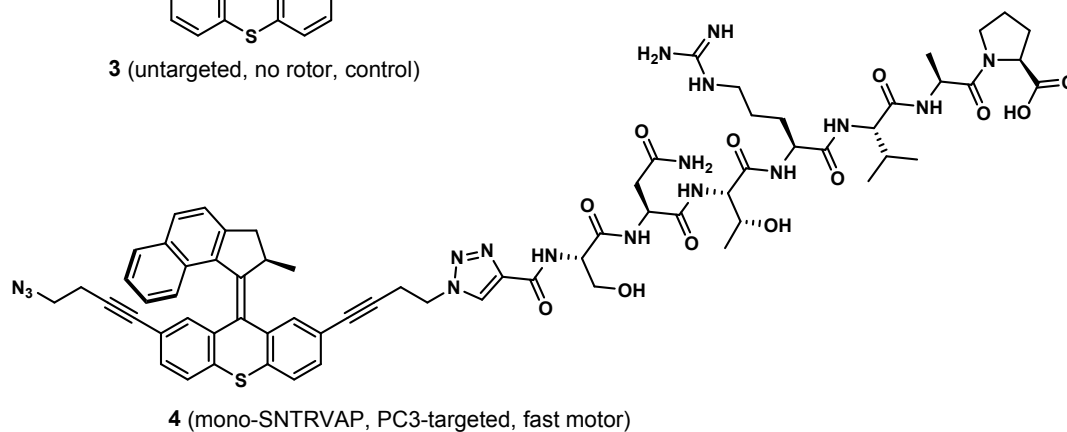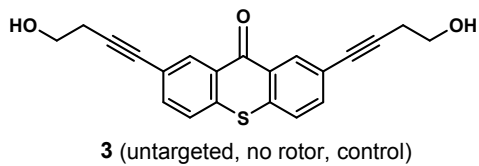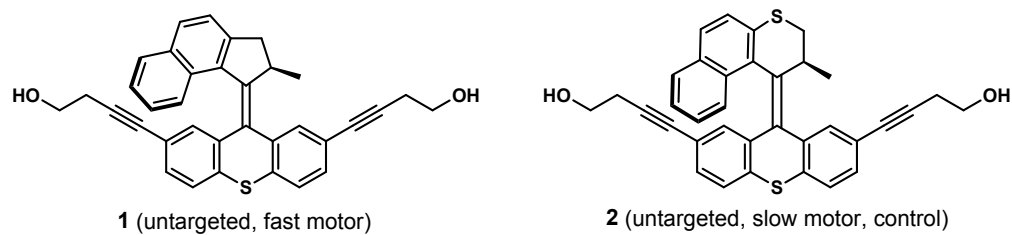ical structures of MNMs and control structures. MNM **1** is the fast untargeted motor where the rotor rotates at 2–3 MHz upon activation. MNM **2** is a slow rotor that serves as a control with rotation at 1.8 revolutions per hour when activated with 355–365-nm light at a temperature of 60 °C, but undergoes only *cis–trans* isomerization around the rotor–stator double bond at room temperature. MNM **3** has a stator segment but no rotor; this serves as a control molecule. MNM **4** is mono-functionalized with the peptide SNTRVAP to bind to the 78-kDa glucose-regulated protein (GRP78), which targets castrate-resistant osteogenic prostate cancer receptors on PC3 human prostate cancer cells. MNM **5** bears the peptide DMPGTVLP sequence which targets the human breast adenocarcinoma cell line MCF7. The syntheses are described in the Supporting Information with the NMR characterization data. MNM **6** bears two fluorescent Cy-5 addends for tracking in synthetic bilayer vesicles.

Results/Discussion

Our cell exposure approach uses two protocols that we previously standardized:[1] in Method A the MNMs are loaded into the cell media and the imaging is initiated within 5 min to 24 h. In Method B, the MNMs are loaded into the cell media, incubated for 30 min to 24 h, then washed

three times with fresh MNM-free media before imaging. In all experiments, MNMs are used as a stock solution at 1.00 μM with total dimethyl sulfoxide (DMSO) concentration of 0.1% in the final cell media in order to avoid unwanted cell membrane permeabilization; the DMSO being required for solubility of the organic MNMs. As detailed in our previous communication,[1] we have studied a wide range of concentrations 100 nM-10 μM. We have found this concentration range suitable and non-toxic. However, our reasoning to settle on a 1 μM working concentration is due to experimental considerations with respect to suitable dilution and compatibility with our previously determined and used imaging sequence. Using lower concentrations have prolonged our imaging sequences and provided (due to simple dilution effects) higher errors in precisely establishing the time of light activated nanomachine induced necrosis. Propidium iodide (PI, total concentration 0.10 μM) was introduced to the cell medium immediately prior to the time-dependent standardized imaging. PI is a fluorescent intercalating agent that is not internalized by healthy cells, and it is non-toxic as shown by our earlier MNM-free controls. Upon membrane disruption by nanomechanical action of the MNMs, PI enters the cell, travels to RNA- and DNA-rich sites where it intercalates and its excitation maximum subsequently displays ~30 nm bathochromic shift (from 535 to 565 nm) accompanied by a parallel hypsochromic emission maximum shift (from 617 nm to 600 nm), with a 10-fold hyperchromic shift or emission intensity increase, consistent with literature-referenced trends.[13] Internalized RNA- and DNA-induced PI fluorescence is detected between 600 and 630 nm upon 532 nm laser excitation, allowing time-dependent 2PE-activated molecular motor-induced cell permeabilization to be confirmed. Further, PI is used to follow membrane damage that is due to 2PE-activated nanomachine activity leading to necrosis. Since the entry of the PI is rapid compared to the time of cell division, the cell has insufficient time to follow apoptotic programmed cell death. This was earlier confirmed using Annexin V, an

apoptosis-specific stain where no relevant fluorescence from this dye was observed throughout the course of the experiments.[1] Necrosis was recorded by extracellular membrane rupture, blebbing, and homogenous cytosolic auto-fluorescence, indicating loss of cellular organelle boundaries. Conversely, visual signs of apoptosis were not seen but they would involve cell shriveling and then detachment from the substrate followed by fragmentation. This has been verified by using Annexin V as detailed above.

We first demonstrated successful precision and targeted-selective cell killing by the MNMs using a confocal UV source, underscoring the ability to use directed MNM activation for precision, coupled with peptide addends for cell-surface targeting. Those underpinning UV-source studies are described in Figures S1-3. In the experiments here, the rationale behind our multiphoton excitation approach is that two (and higher) photon activation is inherently confocal stemming from the high spatial isolation of the excitation event.[2,14,15] MNM activation by 2PE will only occur in a diminutive diffraction-limited 3D voxel (focal spot, 230 nm lateral and 660 nm axial resolution calculated at 1.4NA using 710 nm excitation),[2] allowing photo-manipulation in strongly scattering tissue affording high precision 3D nanomachine activation. As with all commercial laser scanning confocal microscope (LSCM) systems, lateral xy region of interest (ROI) precision is achieved using a galvanometric laser beam. The beam is for scanning and selectively activating the MNMs in the studied field of view (FOV) with inherent sub-diffraction limited axial (z) precision and enhanced optical penetration.[16,17]

Since the nanomachines reported and studied here are non-fluorescent, tracking and visualization by flow cytometry to verify uptake is not possible. Studying the effect of light (multi-photon) induced cell death is perfectly feasible using flow cytometry and PI. However, the cells need to be plated before being irradiated with a multiphoton source through a microscope to allow

the effect of the nanomachines to be manifested. Following light activation, the cells would need to be detached, treated with PI and analyzed by flow cytometry. The added steps would introduce more experimental errors. In addition, scaling this activation up to a flow cell and the required volumes is experimentally challenging.

Alternatively, the cells could be studied using PI cassettes using a ChemoMetec cell counter since it has been used to determine unactivated (light suppressed) nanomachine toxicity (please refer to Supporting Information). However, in this case the process has been simplified and the need for auxiliary equipment was eliminated. We conducted the studies using the microscope itself by studying randomly selected field of views using repeats of different cell cohorts. This has provided a statistically significant number of independent repeats that has been detailed as a method in our prior work[1] and in the present Supporting Information.

In the MPE actuation experiments, we used non-tagged motor molecules as well as those peptide-attached motor molecules. We have verified experimentally that the unsubstituted nanomachines do not show significant aggregation in aqueous solution through monitoring their weak fluorescence. It is assumed that self-aggregation would lead to "self" quenching and deactivation of rotation and residual fluorescence *via* exciplex formation and non-radiative decay processes. No self-aggregation was observed in the studied concentration range (up to 10 μM). In our case the MNMs are solubilized in cell media by associated interaction with the proteins and small biomolecules present. These interactions have also been found to be non-disruptive with respect to rotation or residual autofluorescence.

With respect to the targeted MNMs, the protein linkers on the MNMs aid water solubility and they have been found not to self-aggregate at the applied 1 μM total MNM concentration. We have only observed visible self-aggregation, possible due to the protein linker interaction at

concentrations over 100 μM.

The 2PE cross-section determination studies,[18-21] using residual MNM fluorescence measurements,[12] suggest that the reported MNMs possess high enough 2PE cross sections (σ^2_1= 10.3 GM, σ^2_2= 7.1 GM, σ^2_3= 3.7 GM, σ^2_4= 9.1 GM, σ^2_5= 8.9 GM for each of the molecules **1-5**, respectively) to be activated and studied using suitable wavelength IR laser light with our established target lines (Figure 2 and Figure S4).
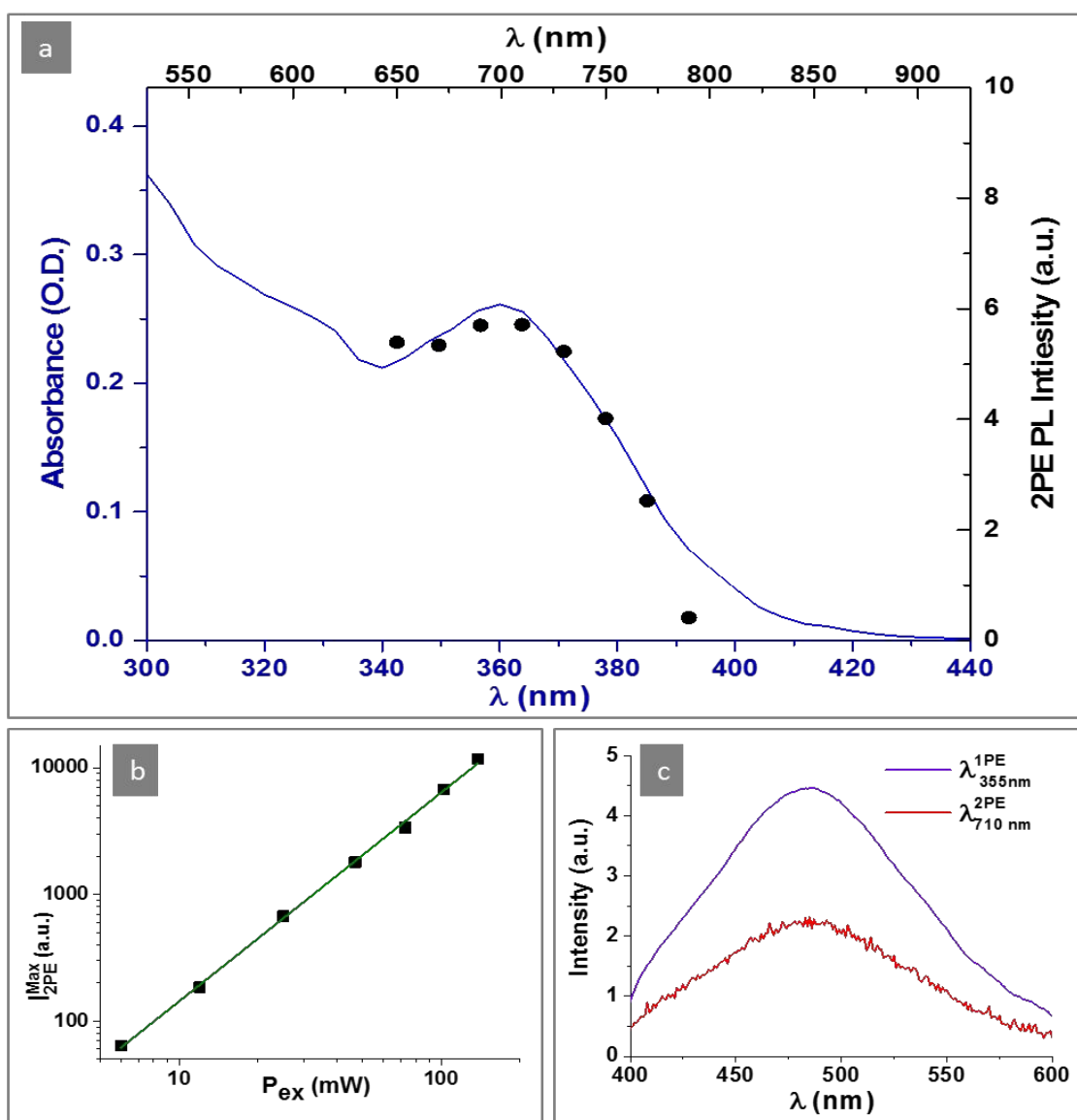
Figure 2. Optical studies to assess 2PE NIR excitation efficacy of MNM 1. (a) One photon absorption (blue) and two (●) photon excitation spectrum (λ_{em} = 500 nm) plot of **1** (Φ_f = 3.7 x 10^{-3}, Σ = 15400 dm^3 mol^{-1} cm^{-1}). (b) Excitation power dependency (green, ■) of the photo luminescence (PL) intensity (10^{-50} cm$^4 \cdot$s photon^{-1}), slope 1.96 ± 0.1 in DMSO. (c) 1PE (purple, λ_{ex} = 355 nm) and 2PE (red, λ_{ex} = 710 nm) emission spectrum of MNM **1**.

Using a 2PE-enabled confocal microscope (microscope setup and imaging parameters are detailed in the SI), we observe a series of 2PE activations using MNMs **1**, with **2** and **3** as controls, and cell-targeted **4** and **5**. All experiments were executed using a standardized constant photon flux/voxel (~2 x 10^{29} cm^{-2} s). These parameters have been maintained by carefully pairing and adjusting the objective magnification, numerical aperture (NA), laser power and line scan speed accumulation and averaging.

To further show that 2PE has very high axial precision in MNM activation, single-cell-precision necrosis is induced in a tissue sample. Confluent PC3 cells are treated with **4** using Method B. We initially identified preselected foci of cells using transmission and single photon fluorescence microscopy (CellMask DeepRed, CMDR, 100 nM, 30 min pre-incubation) with 3D z-stack scans revealing cell arrangements and orientations where one cell occupies higher axial dimension (z) than the height of the voxel size declared by the applied objective magnification and the NA for the 2PE system (Figure 3a). In these experiments the plane of 2PE activation/excitation is at least two axial units (d$_z$ = 890 nm, λ_{ex} = 710 nm, 0.75 NA) higher than the adjacent cell, and the entire FOV is radiated with NIR light in a xy raster pattern maintaining constant imaging parameters. Selective 3D MNM activation has proven to be successful in all cases despite the fact that all cells in the FOV have surface-bound MNMs and have been scanned by NIR light. Only

cells occupying space in the axial plane of activation showed subsequent PI uptake (Figure 3b)

confirming selective high axial precision-induced necrosis. Furthermore, PI has been visualized

using single photon LSCM in a whole cell 3D xyz manner comprising five distinct confocal axial

planes to cover the total height of the studied cell foci.
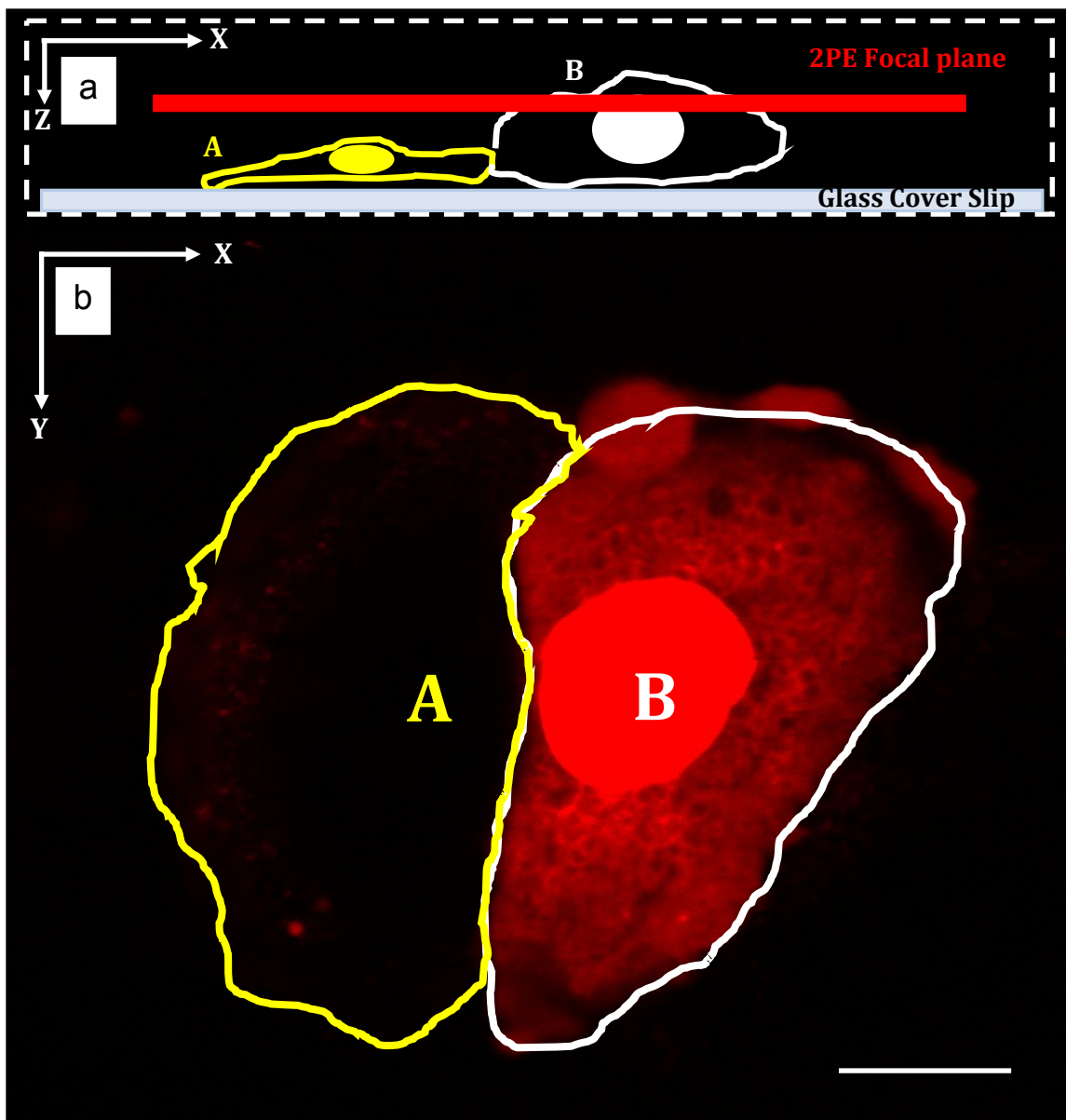
Figure 3. Demonstration of z-dimension precision in cell killing using 2PE NIR. (a) Schematic

representation of a selected PC3 cell focal plane with surface bound MNMs with high axial

11

precision MNM 2PE activation (710-720 nm). (b) Full FOV image of PC3 cells with **4** (Method B) displaying overlaid z-stack of PI (100 nM red, λ_{ex} = 543 nm, λ_{em} = 610–630 nm, 0.2 mW) uptake confirming high precision 3-dimensional selective-induced necrosis, with blebbing, only by the cell occupying space in the selective focal plane of 2PE activation (710 nm, 65 mW, 80 MHz, 100 fs, x20 0.75NA objective). These powers are referenced to the laser setting; the actual excision energy is not calculated since it is specific to NA and scan speed. Scale bar is 20 μm.

The 2PE microscopy studies using MNMs **1** and **4** and both NIH3T3 and PC3 cell lines have validated the feasibility of using cell type and pathophysiological condition-specific MNMs. While NIR light activation is deemed biologically safer since its phototoxicity is orders of magnitude lower than when using UV light,[22] at this level of prolonged NIR exposure we establish that blank cells display an onset of necrosis confirmed by PI internalization at 20 min. This is attributed to the NIR-induced heating of the sample at the focal voxel. When the untargeted MNM **1** is introduced, both NIH3T3 and PC3 cells displayed early onset of PI-signaled cell necrosis starting at 3 min which is >600% acceleration in comparison to the 50% acceleration (5 min MNM + UV-induced necrosis *vs* 10 min UV-alone-induced necrosis) achieved using our former UV activation method[1] (Table S2). The level of 2PE-activated acceleration in the observed rate of necrosis has also been maintained using the PC3-selective **4** MNM using both Methods A and B (Figure 4, Table S3). Figure S5 shows control experiments using the slow motor MNM **2** and the rotorless **3** showing no enhancement in the cell death rate, suggesting that reactive oxygen species (ROS) generation is not the reason for MNM-enhanced cellular death rates upon 2PE activation.
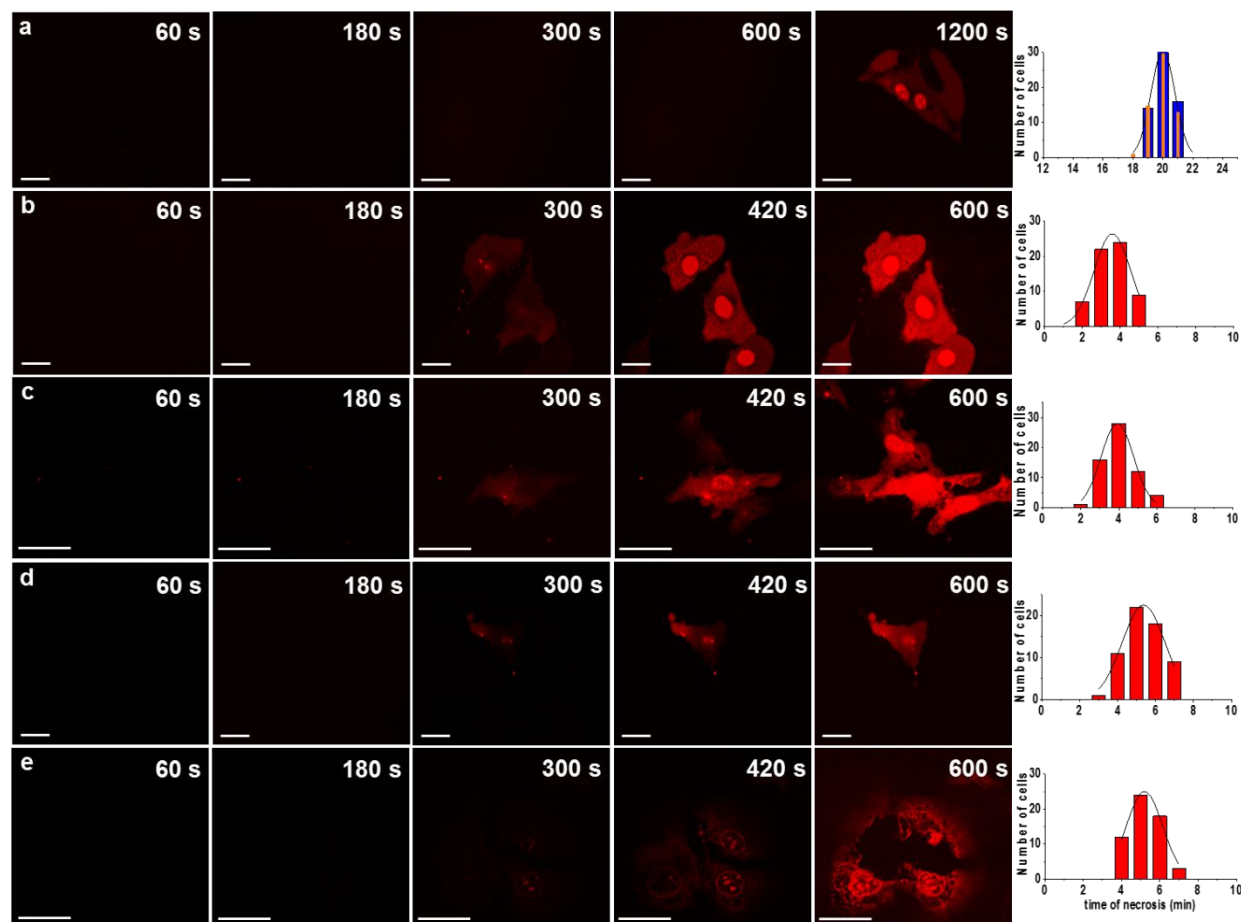
Figure 4. Enhanced killing of NIH3T3 and PC3 cells using 2PE of MNMs 1 and 4. Full FOV

xy as a function of time imaging depicting PI (100 nM red, λ_{ex} = 543 nm, λ_{em} = 610–630 nm, 0.2

mW) internalization and MNM-induced morphological changes and necrotic cell death upon 2PE

activation (710 nm, 65 mW, x20 0.75 NA objective). The histograms at the right of each row

show the number of cells and their range of necrosis times. (a) MNM-free PC3 (blue bars in plot)

and NIH3T3 (orange bars in plot) cells with activation only by 2PE, no nanomachines, to establish

control necrotic rate. Standard deviation (s.d.) = 0.9. (b) NIH3T3 cells with the introduction of **1**,

Method A (1 μM, 5 min incubation), s.d. = 1.4. (c) PC3 cells with **1**, Method A (1 μM, 5 min

incubation), s.d. = 0.9. (d) PC3 cells with **4**, Method A (1 μM, 5 min pre-incubation), s.d. = 1.2.

(e) PC3 cells with **4** Method B (1 μM, 30 min pre-incubation prior to wash), s.d. = 1.0. Scale bars

13

represent 20 μm.

Upon successful identification of the DMPGTVLP cell-surface recognition peptide sequence as a promising target vector for human breast adenocarcinoma cell line MCF7,[23] we synthesized **5** to target MCF7 cells. HeLa cells are used as the non-targeted control. 2PE NIR-activation of MNM **5** results in accelerated necrosis in as early as 3 min regardless of the applied loading Method A or B. Crucially, studying the effect of 2PE-MNM-induced necrosis using HeLa cells, the rate of acceleration is only observed when Method A is used. When Method B is used with HeLa cells, no acceleration in 2PE-induced necrotic cell death times is observed (Figure 5, Table S3 and Figure S5) since all the MNMs had been washed from those cells. This confirms the targeted-selectivity using the DMPGTVLP cell-surface recognition peptide sequence toward the MCF7 cell line.
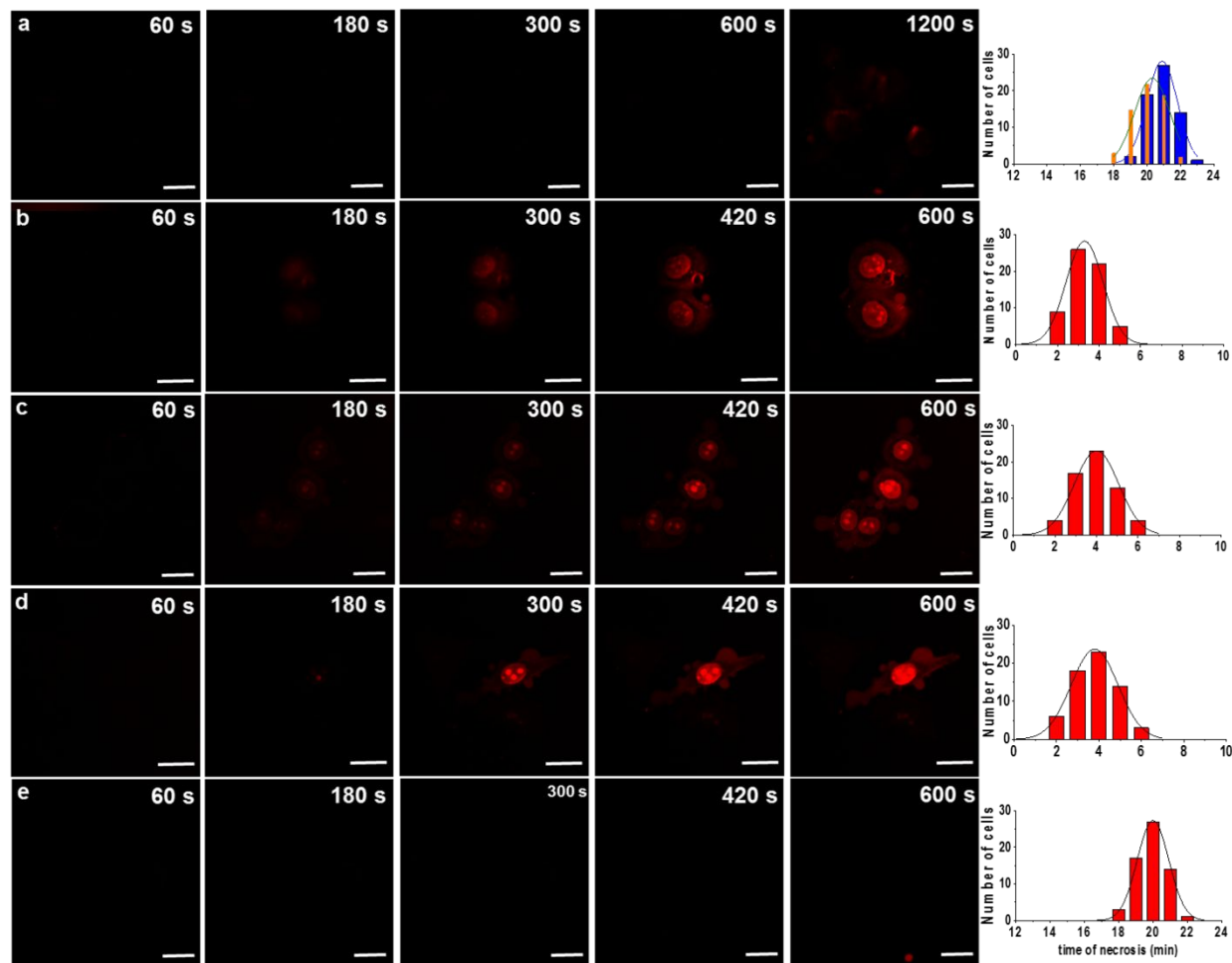
Figure 5. **Enhanced targeted killing of MCF7 over HeLa cells using 2PE of MNM 5.** Full FOV

xy as a function of time imaging depicting PI (100 nM red, λ_{ex} = 543 nm, λ_{em} = 610–630 nm, 0.2

mW) internalization and MNM-induced morphological changes and necrotic cell death upon 2PE

activation (710 nm, 65 mW, x20 0.75 NA objective). (a) MNM-free MCF7 (cell images shown

and blue bars in plot) and HeLa (orange bars in plot, cell images not shown) cells with activation

only by 2PE, no nanomachines, to establish control necrotic rate, s.d. = 1.1 (b) MCF7 cells with **5**

using Method A (1 µM, 5 min incubation), s.d. = 1.2. (c) MCF7 cells with **5** using Method B (1

µM, 30 min pre-incubation prior to wash), s.d. = 1.2. (d) HeLa cells with **5** using Method A (1

µM, 5 min incubation), s.d. = 1.2. (e) HeLa cells with **5** using Method B (1 µM, 30 min pre-

incubation prior to wash), s.d. = 1.0. Scale bars represent 20 µm.

15

Cells are highly complex entities that might have confounding features rending a misinterpretation of the mechanical effects proposed here. Therefore, we sought to use a more simple control system as a verification. To that end, synthetic bilayer vesicles (see Supplemental for details of preparation and excitation) were studied using MNM **6**.[1] The MNMs were used to release boron-dipyrromethene (BODIPY) dyes that were co-encapsulated with the MNMs in the vesicles. Interestingly, the hydrophilic Cy-5 addends on MNM **6** might associate with the bilayer surface.

The vesicles were first repeatedly scanned by using a Ti:Sapphire laser beam (730 nm, ~140 fs, focused to a FWHM of 350 nm, 9.0 mW) at top half of the image (Figure 6a). The fluorescence image (signal from BODIPY) was then acquired using the same confocal fluorescence microscope with a 514 nm laser at 47 kW/cm^2. During each NIR laser scanning, the total exposure time of the vesicle to the NIR laser was estimated to be 50 ms. From Figure 6a, in MNM-**6**-containing vesicles, the intensity from BODIPY decreased significantly after laser exposure (Figure 6a, top half of the images). In the same images, the area that was not exposed to the laser beam (Figure 6a, bottom half of the images) showed a much slower intensity drop. That there was an intensity drop at all is likely due to photobleaching by the near IR laser and the fluorescence excitation laser. Figure 6b shows the results from a BODIPY-containing vesicle that had no co-encapsulated MNMs, hence there was little diminution of the BODIPY-based signal over the same time period. The time-evolution of the vesicle intensities are shown in Figure 6c while the MNM-free analogues are plotted in Figure 6d. This experiment shows that the intensity drop of BODIPY is caused by the releasing of BODIPY from the vesicle, suggesting nanomechanical disruption of the vesicle bilayer membranes by the MNMs.
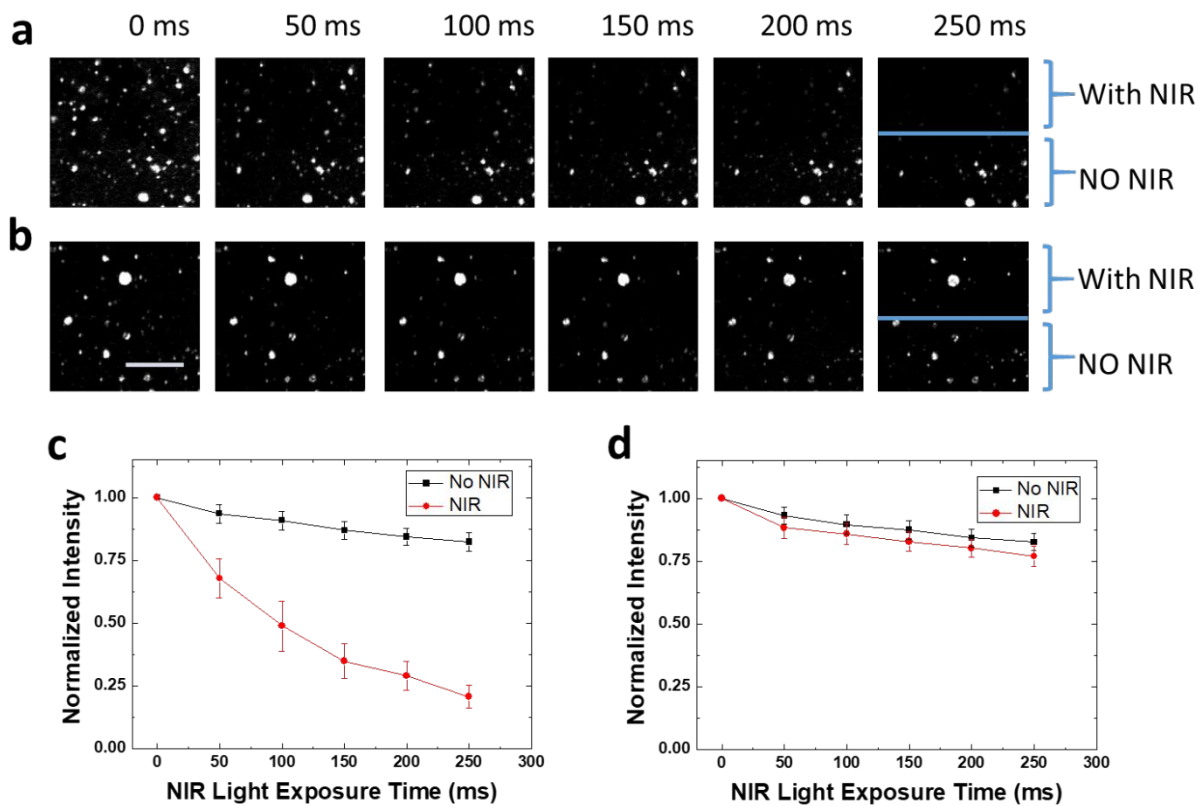
Figure 6. 2PE-actuation of MNM 6 co-encapsulated with BODIPY in synthetic bilayer vesicles. The images were acquired from the BODIPY signal using a confocal fluorescence microscope at 514 nm excitation. Scale bar: 8 μm. (a) The vesicles contain 20 nM BODIPY plus 1.0 nM MNM **6**. Only the top half of the image, as indicated by the blue line, was scanned with the NIR laser, which shows a decrease of BODIPY intensity. The lower half of the image shows a much slower decrease of BODIPY intensity, likely declining because of photobleaching induced by the NIR laser and the excitation laser. The NIR exposure times are listed at the top of the images. (b) Control experiments with vesicles containing 20 nM BODIPY only. Again, only the top half of the image were scanned with the NIR laser. (c) Normalized vesicle intensity (from BODIPY) decay after being exposed to the NIR laser for excitation of the MNMs. The error bar was from 15

17

vesicles on four different sample slides. (d) Normalized vesicle intensity for the control experiments (BODIPY encapsulated only) without MNM **6**.

Conclusions

Using a series of light-activated and also cell-type-targeted MNMs, we demonstrate the use of molecular mechanical action to open cellular membranes and expedite cell death. This has been done using biologically safe multi-photon excitation in the NIR domain. The ~200 nm optical precision of 2PE means that one diffraction limited spot that activates the MNMs will be sufficient to rupture the cell membrane and trigger death by necrosis. The initiated early necrotic stage, therefore, should be further exploited and accelerated in a whole-cell manner where the MNMs can destroy and further break down intracellular biological matter of the targeted cell. By additional MNM-induced destruction of components like chromatin, deleterious invasion into neighboring cells is less likely, thereby slowing metastasis. We are further modifying the MNM structure to induce a shift in the absorption thereby providing biologically acceptable visible excitation, or to increase of the 2PE cross section and excitation wavelength in the NIR. The families of cell-type-specific MNMs are also to be expanded for skin, oral and gastrointestinal cancer cell lines where light-activation is amenable.[24,25] This could be a photodynamic therapy using a non-invasive approach that can also be coupled with extremely high 3D optical precision.

Methods/Experimental

Live cell cultures studies

A detailed investigation of the cellular behavior of each complex was conducted using NIH3T3, PC3, HeLa and MCF7 cell lines using fluorescence and laser scanning confocal

18

microscopy. These cell lines were sourced from ATCC (NIH 3T3 CRL-1658, PC3 CRL-1435, Hela CRM-CCL-2 and MCF7 HTB-22) and have been established and maintained in a category 2 cell culture facility according to established standardized protocol for 12 months; they have been periodically monitored for mycoplasma contamination.[26] Cells were maintained in exponential growth as monolayers in F-12/DMEM (Dulbecco's Modified Eagle Medium) 1:1 that was supplemented with 10% fetal bovine serum (FBS). Cells were grown in 75 cm^2 plastic culture flasks, with no prior surface treatment. Cultures were incubated at 37 °C, 10% average humidity and 5% (v/v) CO_2. Cells were harvested by treatment with 0.25% (v/v) trypsin solution for 5 min at 37 ºC. Cell suspensions were pelleted by centrifugation at 1000 rpm for 3 min, and were re-suspended in fresh medium by repeated aspiration with a sterile plastic pipette. Microscopy cells were seeded in untreated iBibi 100 μL live cell channels and allowed to grow to 40% to 60% confluence, at 37 ºC in 5% CO_2. At this stage, the medium was replaced and cells were treated with the studied nanomachines and co-stains as appropriate, with 0.1 % DMSO (as detailed above) present in the final imaging medium. For live cell imaging, DMEM/F12 media (10% FBS) lacking phenol red was used from this point onwards. Following incubation, where Method B was used, the channels were washed with live cell imaging media and imaged using a purpose build incubator housing the microscope maintaining 37 ºC, 5% CO_2 and 10% humidity.

All live cell imaging experiments used either NIH 3T3 mouse skin fibroblast cells, PC-3 cells, a grade 3 human prostate adenocarcinoma, HeLa cells, a human cervical cancer, or human breast mammary gland cancer cells (MCF7). These are all well-studied cell lines with discrete morphological compositions. Two previously described[1] experimental methods were used: (Method A) the molecular motors were loaded into the cell media and the imaging was initiated within 5 min to 24 h, or (Method B) the molecular motors were loaded into the cell media,

incubated for 30 min to 24 h, then washed three times with fresh molecular motor-free media before imaging. Each molecular machine was used as a stock solution at 0.10 to 1.00 µM with total dimethyl sulfoxide (DMSO) concentrations not exceeding 0.1% in the final cell media in order to avoid unwanted cell membrane permeabilization; the DMSO being required for solubility of the organic nanomachines. Note that all loading experiments are carried out in a light-suppressed manner and the possibility of induced or accelerated uptake due to interaction between the molecular motors and the applied co-stain has been eliminated using a series of individual and reversed loading experiments.

To further confirm the molecular mechanical opening and subsequent permeabilization of the membrane, a dye was added to the cell medium to assess its exogenous entry into the cells that might be afforded by molecular mechanical action. Using our selected cell types and **3**, PI, total concentration 100 nM, was introduced to the cell medium immediately prior to the time-dependent standardized imaging sequence. PI is a fluorescent intercalating agent that is not internalized by healthy cells, and it is non-toxic as shown by our molecular machine-free controls. Upon membrane disruption by molecular mechanical action of **3** (Figure 3e), PI enters the cell, travels to RNA- and DNA-rich areas where it intercalates and its excitation maximum subsequently displays ~30 nm bathochromic shift (from 535 to 565 nm) accompanied by a parallel hypsochromic emission maximum shift (from 617 nm to 600 nm), consistent with literature-noted trends. Although PI's molar extinction coefficient is relatively low compared to other organic cell dyes, upon intercalation, its red fluorescence emission intensity increases by >10x, thereby becoming a suitable counter-stain to assess and establish the onset of UV-induced necrosis. In light of its favorable spectroscopic properties, no major alteration of the experimental parameters are needed other than exchange of the 488 nm laser line, used to generate transmission images, to 543

nm (0.2 mW, also confirmed to be non-disruptive to cells). Internalized RNA- and DNA-induced

PI fluorescence is detected between 600 and 630 nm allowing time-dependent light-activated

molecular motor-induced cell permeabilization to be confirmed. Further, PI was used to follow

membrane damage that is due to UV-activated nanomachine activity leading to necrotic cell death.

Since the entry of the PI is on a relatively short time scale compared to the time of cell division,

the cell has insufficient time to adopt programmed cell death (apoptosis). This has been confirmed

using Annexin V, an apoptosis-specific stain where no relevant fluorescence from this dye has

been observed throughout the course of the experiments.

In co-culture experiments cell types were cultured individually with selected cell types

individually stained before culture mixing using the common cell wall stain Cell Mask Deep Red

(200 nM, 30 mins, λex = 633 nm, λem = 650–700 nm) that is known to be internalising into all

our studied cell lines in an unselective and nontoxic manner.[27] This has provided the foundation

to a method that has been developed in house with both apoptotic and necrotic cell death tested

and found that rather than disrupting natural cell homeostasis the CMDR have been slowly

excreted by the cells after 48 h before cell division as there was no evidence of daughter cells

containing CMDR. It is important to emphasize that CMDR has found to be photobleached

throughout our experiments as a result of the incorporated parallel UV exposure sequence to

activate MNMs, however it is a suitable method to identify different co-culture cells when the

studied FOV has been established. As a result of incorporating CMDR visualisation into our

previously established imaging/activation sequence[1] to study MNMs induced accelerated

necrosis has been extended to a one frame triple channel imaging sequence that totals 20 s.

Cell toxicity was determined using a ChemoMetec A/S NucleoCounter3000-Flexicyte

instrument with Via1-cassette cell viability cartridge using the cell stain Acridine Orange for cell

detection, and the nucleic acid stain DAPI for detecting non-viable cells and Annexin V for the detection of apoptosis. See Figure S6 for cell viability values. In cellular uptake studies, cells were seeded in 6-well plates and allowed to grow to 80% to 100% confluence at 37 ºC in 5% CO_2. Culture medium was then replaced with culture medium containing 0.1% DMSO with individual nanomachines for 24 h at 1.00 µM. All cell colonies bearing nanomachines displayed 92 ± 5% viability; the control blank cells were established at 95 ± 3% viability. In addition to 0.1% DMSO being used for molecular machine introduction, all washing solutions also contained 0.1% DMSO. At this concentration DMSO does not affect the cells; this was determined by control experiments using all imaged cell lines cultured in DMSO-free and 0.1% DMSO-containing cell media while establishing the initial control UV-induced cell death parameters.

Similar toxicity measurements were executed prior to selective cell specificity experiments using the commercial cell wall stain Cell Mask Deep Red (200 nM, 30 min loading and subsequent up to 48 h retention) To confirm the non-activated low toxicity of these molecular machines and all applied counter dies, all live cell imaging samples with all three studied cell lines were re-incubated, using Method A, in the dark and re-imaged using only transmission microscopy. These experiments confirmed that all previously non-UV-exposed cells, regardless of the cell line studied, still proliferated in the presence of the molecular motor stock solutions for up to 72 h using visible light at a pre-set time point to assess cell morphological changes along with viability and vitality.

Two-photon emission (2PE) cross section determination[18,19,28]

The theoretical framework and experimental protocol for 2PE measurements has been outlined by Webb *et al*.[20,29] In this approach the ratio of the reference and sample 2PE-PL (Photo

Luminescence) is given by eq 1:

$$\frac{\sigma_2^S \cdot \phi^S}{\sigma_2^R \cdot \phi^R} = \frac{C_R \cdot n_S \cdot F^S(\lambda)}{C_S \cdot n_R \cdot F^R(\lambda)} \text{ (eq 1)}$$

where ϕ is the total emission quantum yield of the compound, composite PL of respective nanomachine for ϕ^S, C is the concentration, n the refractive index and $F(\lambda)$ is the integrated PL spectrum. In these experiments we have ensured that the excitation flux and excitation wavelengths are the same for both sample and reference.

Two photon excitation source consisted of a precompensated 80 MHz Ti:Sapphire laser (Chameleon™ Vision II, Coherent) producing near infra red optical pulses with a temporal width of ~70 fs (FWHM) in the selected wavelength range 650 – 780 nm (and 760 nm for reference). The excitation light was focused into the sample solution using a Leica HC PL APO 20x/0.75 IMM CORR CS2 objective. The emission was subsequently collected using a 90° geometry, with a 395 nm dichroic mirror, to allow epifluorescence detection using a fiber coupled CCD spectrograph (Ocean Optics Maya2000 Pro, 400-800, 1000 averaged spectra of 7.2 ms rolling acquisition) with a 800 mm fiber core. The output power was monitored using a photodiode with a known response curve and a free standing power meter. The intensity of the excitation light was modulated using a ND filter with a continuous grey scaling (Edmund optics) mounted on a translation stage. Typical average excitation power was 5-*1*50 mW corresponding to pulse energies of 1.25 – 37.5 nJ/pulse. In our previous and current studies, we have done extensive controls using molecules with similar structures (*e.g.* slow motors) in both live cell experiments and synthetic lipids using NIR light and UV light. The results show that opening of the bilipid membrane is unique to fast motors, indicating that (1) the mechanical motion is the main reason for the opening, and (2) photodegradation is not the main reason, and may not be significant in these studies. Photodegradation is an important

23

issue for the application of these molecular machines. We are currently carrying out systematic studies in their *in vivo* applications. Spectra from the CCD spectrograph were corrected for background and spectral response. The TTL signal for the detector operating at a 100 Hz collection sequence with a 7.2 ms rolling emission colelction sequence was synchronised with the intial pulse form the laser cavity dumper driver.

Two photon absorption cross sections where calculated using a reference: Fluorescein/NaOH, at an excitation wavelength of 760 nm.[30] The parameters used for Fluorescein in obtaining the respective nanomachine crossection where; a two photon cross section of $\sigma 2 = 36$ GM and a fluorescence quantum yield of f = 0.9.[ref 29] A validation experiment was performed using Rhodamine B/Methanol and Fluorescein/NaOH. In this experiment the ratio of the literature parameters eq 2,[20]

$$\frac{\sigma_2^{Rh} \cdot \phi_{Rh}}{\sigma_2^{Fl} \cdot \phi_{Fl}} = R_{lit} \text{ (eq 2)}$$

Was compared to the experimentally obtained ratio eq 3,

$$\frac{C_{Fl} \cdot n_{Rh} \cdot F_{Rh}(\lambda)}{C_{Rh} \cdot n_{Fl} \cdot F_{Fl}(\lambda)} = R_{exp} \text{ (eq 3)}$$

where C is the concentrations, n the refractive index and $F(\lambda)$ is the integrated emission. This comparison returned the same ratios, $R_{lit} \approx R_{exp}$ which in turn confirms that our experimental procedures are correct.

PhMoNa and Multi-Photon equipment

As per our previous publication all single photon microcopy live cell experiments have been performed on the above detailed custom built PhMoNa[31] system based on a Leica SP5 II (DMI6000 inverted chassis) LSCM platform operating with a fiber-coupled 355 nm Coherent laser (Nd:YAG 3rd Harmonic, 80 mW) for UV activation of the motor. The modular PhMoNa[31]

24

technique is based on a laser scanning confocal microscope (LSCM) harnessing spatially modulated illumination intensities, using an *in situ* generated raster-scanned standing wave excitation beam optical grid pattern. Such an approach allows experimental resolution in both lateral and axial domains to be improved by at least a factor of 2 (x,y = 62 nm, z = 188 nm @ 355 nm Ex 63x 1.40NA, 100 Hz/line, 200 nJ/voxel dwell time) and is free from time-consuming post-image processing deconvolution algorithms. Steady state fluorescence images were recorded using the PhMoNa enhanced Leica SP5 II LSCM confocal microscope equipped with a HCX PL APO 63x/1.40 NA LambdaBlue Oil immersion objective. Data were collected using 2x digital magnification at 100 Hz/line scan speed (4-line average, bidirectional scanning) at 355 nm (3rd harmonic NdYAG laser, set at 20 mW, 400 nJ/voxel total dwell time). In order to achieve excitation with maximal probe emission, the microscope was equipped with a triple channel imaging detector, comprising a conventional PMT systems and two HyD hybrid avalanche photodiode detectors. The latter parts of the detection system, when operated in the BrightRed mode, is capable of improving imaging sensitivity by 25%, reducing signal to noise by a factor of 5. Frame size was determined at 1024 × 1024 pixel, with ×2 digital magnification to ensure illumination flatness of field and 0.6 airy disc unit determining the applied pinhole diameter rendering on voxel to be corresponding to 62 x 62 nm^2 (frame size 125 × 125 μm^2) with a section thickness set at 188 nm (at 355 nm excitation). A HeNe or Ar ion laser was used to aid parallel transmission image capture and when commercially available organelle-specific stains (*e.g.* CMDR™ or PI) were used to corroborate cellular compartmentalization or follow the onset of necrosis or differentiate various co-cultured cell types.

All imaging parameters are kept constant across experiments. This includes voxel size, laser power, line speed and averaging sequences, unless otherwise noted. The accuracy and errors

associated with the establishment of accelerated necrosis is one frame dual channel imaging sequence that totals 15 s. This imaging sequence has been carefully established using untreated live cells. The optimized imaging parameters allow appropriately high scanning speed to follow natural homeostatic events and identify any induced morphological or fluorescent signal localization change. Meanwhile, they also allow sufficiently long integration time for each pixel so an adequate amount of photon signals can be collected. In order to satisfy the Nyquist sampling criteria, the pixel size is set as 1/5 of the laser spot size. The images were acquired using a bidirectional 2-line averaging sequence, which gives minimal dead time (< 1 ms) between line scanning. The image size FOV was adjusted to 100×100 μm in order to study 1 to 3 cells simultaneously. Each individual experiment was repeated 3 times on triplicate slides. On each slide, at least 5 well-separated areas were imaged.

As an initial control experiment to establish the UV-induced cell toxicity threshold, while mitigating voxel exposure and ensuring sufficient laser dwell time, an imaging sequence has been established to monitor cell morphological and physiological changes as a function of time. The applied 100 Hz detection sequence was based on a bidirectional dual-channel continuous scanning method where a minimalistic non-damaging visible laser light (458 nm, 0.2 mW) is used in conjunction with the above detailed UV exposure. This is set as a 2 line/scan accumulation parallel acquisition sequence that is recorded as a function of time. Studied channels correspond to transmission images and UV-induced mitochondrial auto-fluorescence detected at 460 to 550 nm.

Multiphoton microscopy has been conducted on three instruments at two locations. At Durham (Department of Biosciences) a Nikon E600 upright microscope equipped with a BioRad MicroRadiance 2000 Multiphoton head coupled to a Spectra-Physics MaiTai tunable (710-950 nm, 80 mW @ 720 nm, 80 MHz, 100 fs) multiphoton and a 543 nm (1 mW, 560 nm LP) HeNe

laser using a x60 1.4NA water immersion IR objective (operating at 166 lines/s scan speed 128 ×

128 pixel and 512 × 512 pixel FOV for MP nanomachine activation and PI imaging respectively)

has been used. At Rice (Baylor College of Medicine, BCM) a Leica SP8 mutiphoton microscope

(DM5000 CS upright chassis) equipped with a quad HyD NDD Leica TCS MP scan head coupled

to a Coherent Chameleon tunable (680 – 1050 nm, 65 mW @ 710 nm, 80 MHz, 100 fs)

multiphoton and a 561 nm (2mW, AOTF 580 -700 nm) DPSS laser using a x20 0.95NA IMM

CORR objective (operating at 100 Hz scan speed with 2 line accumulation uni-directional 1024 ×

1024 pixel FOV for sequential MP nanomachine activation and PI imaging) has been used. 2PE

activation of the MNMs were achieved using an optimized x3.5 digital zoom to provide a 120 ×

120 μm FOV in order to study 1 to 3 cells simultaneously and provide sufficient continuous NIR

laser scanning with sufficiently long integration time for each pixel so an adequate amount of

photon can be delivered to promote nonlinear MNM activation. Scan speeds for NIR activation

were set at an uni-directional 100 Hz with the above detailed scan settings with quick interruption

of a 400 Hz 561 nm FOV 2 line average bidirectional scan for collecting evidence of PI

internalization to establish the progression of induced necrosis. This later FOV scan took 10 s that

interrupted a sequential set of 60 s long NIR exposures. During our investigation we have also

coupled our existing UV enabled Lecia SP5 II microscope to an identical Coherent Vision II laser

used at BCM using a Leica HC PL APO 20x/0.75 IMM CORR CS2 objective. All experiments

detailed in this manuscript were repeated on all three 2PE microscope setups to achieve 100%

correlation in results (using blank cells and MNM **3**) in time of necrosis a standardized constant

photon flux/voxel (~2 x 10^{29} cm^{-2} s) have been maintained by careful pairing and adjustment of

objective magnification and NA, laser power and line scan speed. This is also an important point

to raise as it validates replicability and suggests that by careful MNM activation method

development the results can be made independent of applied make of both laser and microscopy equipment. All experiments used cell-line-determined culture medium containing 0.1% DMSO. The threshold algorithm to control brightness automated by the BioRad MicroM and Leica LAX software respectively is calculated by the image specific signal-to-noise ratio or it is accessible post image-processing *via* imageJ 1.49h.

Supporting Information The Supporting Information is available free of charge on the ACS Publications Website at DOI:

This includes synthetic methodology, ^{1}H and ^{13}C NMR spectra, additional images and graphs (PDF).

Conflicts of Interest. Rice University owns intellectual property on the use of nanomachines to

28

kill cells. That property is presently unlicensed.

References

[1] García-López, V.; Chen, F.; Nilewski, L. G.; Duret, G.; Aliyan, A.; Kolomeisky, A. B.; Robinson, J. T.; Wang, G.; Pal, R.; Tour, J. M. Molecular Machines Open Cell Membranes. *Nature* **2017**, *548*, 567-572.

[2] Williams, R. M.; Zipfel, W. R.; Webb, W. W. Multiphoton Microscopy in Biological Research. *Curr. Opin. Chem. Biol.* **2001**, *5*, 603–608.

[3] Rubart, M. Two-Photon Microscopy of Cells and Tissue. *Circ. Res.* **2004**, *95*, 1154–1166.

[4] Lakshmanan, S. Gupta, G. K.; Avci, P.; Chandran, R.; Sadasivam, M.; Jorge, A. E. S.; Hamblin, M. R. Physical Energy for Drug Delivery; Poration, Concentration and Activation. *Adv. Drug Delivery Rev.* **2014**, *71*, 98–114.

[5] Xu, T.; Gao, W.; Xu, L.-P.; Zhang, X.; Wang, S. Fuel-Free Synthetic Micro-/Nanomachines. *Adv. Mater.* **2017**, *29*, 1603250.

[6] Findlay, J. A.; Crowley, J. D. Functional Nanomachines: Recent Advances in Synthetic Molecular Machinery. *Tetrahedron Lett.* **2018**, *59*, 334–346.

[7] Kassem, S.; van Leeuwen, T.; Lubbe, A. S.; Wilson, M. R.; Feringa, B. L.; Leigh, D. A. Artificial Molecular Motors. *Chem. Soc. Rev.* **2017**, *46*, 2592–2621.

[8] Kassem, S.; Lee, A. T. L.; Leigh, D. A.; Marcos, V.; Palmer, L. I.; Pisano, S. Stereodivergent Synthesis with a Programmable Molecular Machine. *Nature* **2017**, *549*, 374-378.

[9] Peng, F.; Tu, Y.; Wilson, D. A. Micro/Nanomotors Towards *in vivo* Application: Cell, Tissue and Biofluid. *Chem. Soc. Rev.* **2017**, *46*, 5289–5310.

[10] Watson, M. A.; Cockroft, S. L. Man-Made Molecular Machines: Membrane Bound. *Chem. Soc.*

29

Rev. **2016**, *45*, 6118–6129.

[11] Agarwal, A.; Hess, H. Molecular Motors as Components of Future Medical Devices and Engineered Materials. *J. Nanotechnol. Eng. Med.* **2010**, *1*, 011005.

[12] García-López, V.; Chiang, P. -T.; Chen, F.; Ruan, G.; Martí, A. A.; Kolomeisky, A. B.; Wang, G.; Tour, J. M. Unimolecular Submersible Nanomachines. Synthesis, Actuation, and Monitoring. *Nano Lett.* **2015**, *15*, 8229–8239.

[13] Lecoeur, H. Nuclear Apoptosis Detection by Flow Cytometry: Influence of Endogenous Endonucleases. *Exp. Cell. Res.* **2002**. *277*, 1-14.

[14] Zipfel, W. R.; Williams, R. M.; Webb, W. W. Nonlinear Magic: Multiphoton Microscopy in the Biosciences. *Nat. Biotechnol.* **2003**, *21*, 1369.

[15] Hoover, E. E.; Squier, J. A. Advances in Multiphoton Microscopy Technology. *Nat. Photonics* **2013**, *7*, 93.

[16] So, P. T. C.; Dong, C. Y.; Masters, B. R.; Berland, K. M. Two-Photon Excitation Fluorescence Microscopy. *Annu. Rev. Biomed. Eng.* **2000**, I, 399–429.

[17] Mertz, J. Nonlinear Microscopy: New Techniques and Applications. *Curr. Opin. Neurobiol.* **2004**, *14*, 610–616.

[18] Denk, W.; Strickler, J.; Webb, W. W. Two-Photon Laser Scanning Fluorescence Microscopy. *Science* **1990**, *248*, 73–76.

[19] Göppert-Mayer, M. Über Elementarakte mit Zwei Quantensprüngen. *Ann. Phys.* **1931**, *401*, 273–294.

[20] Xu, C.; Webb, W. W. Measurement of Two-Photon Excitation Cross Sections of Molecular Fluorophores with Data from 690 to 1050 nm. *J. Opt. Soc. Am. B* **1996**, *13*, 481–491.

[21] Saxon, R. P.; Eichler, J. Theoretical Calculation of Two-Photon Absorption Cross Sections in

Atomic Oxygen. *Phys. Rev. A* **1986**, *34*, 199–206.

[22] Denk, W.; Svoboda, K. Photon Upmanship: Why Multiphoton Imaging Is More than a Gimmick. *Neuron* **1997**, *18*, 351–357.

[23] Bedi, D.; Musacchio, T.; Fagbohun, O. A.; Gillespie, J. W.; Deinnocentes, P.; Bird, R. C.; Bookbinder, L.; Torchilin, V. P.; Petrenko, V. A.. Delivery of siRNA into Breast Cancer Cells *via* Phage Fusion Protein-Targeted Liposomes. *Nanomedicine Nanotechnol. Biol. Med.* **2011**, *7*, 315–323.

[24] Bigliardi, P. L.; Rout, B.; Pant, A.; Krishnan-Kutty, V.; Eberle, A. N.; Sriniva, R.; Burkett, B. A.; Bigliardi-Qi, M.. Specific Targeting of Melanotic Cells with Peptide Ligated Photosensitizers for Photodynamic Therapy. *Sci. Rep.* **2017**, *7*, 15750.

[25] Miao, Y.; Quinn, T. P. Peptide-Targeted Radionuclide Therapy for Melanoma. *Crit. Rev. Oncol. Hematol.* **2008**, *67*, 213–228.

[26] Young, L.; Sung, J.; Stacey, G.; Masters, J. R. Detection of Mycoplasma in Cell Cultures. *Nat. Protoc.* **2010**, *5*, 929.

[27] Fenyvesi, F. Réti-Nagy, K.; Bacsó, Z.; Gutay-Tóth, Z.; Malanga, M.; Fenyvesi, E. Szente, L.; Váradi, J.; Yjhelyi, Z.; Fehér, P.; Szabó, G. VecsernyéS, M.; Bácskay, I. Fluorescently Labeled Methyl-*Beta*-Cyclodextrin Enters Intestinal Epithelial Caco-2 Cells by Fluid-Phase Endocytosis. *PLoS ONE* **2014**, *9*, e84856.

[28] Protasenko, V.; Bacinello, D.; Kuno, M. Experimental Determination of the Absorption Cross-Section and Molar Extinction Coefficient of CdSe and CdTe Nanowires. *J. Phys. Chem. B* **2006**, *110*, 25322–25331.

[29] Albota, M. A.; Xu, C.; Webb, W. W. Two-Photon Fluorescence Excitation Cross Sections of Biomolecular Probes from 690 to 960 nm. *Appl. Opt.* **1998**, *37*, 7352–7356.

[30] Palsson, L. -O.; Pal, R.; Murray, B. S.; Parker, D.; Beeby, A. Two-Photon Absorption and Photoluminescence of Europium Based Emissive Probes for Bioactive Systems. *Dalton Trans* **2007**, 5726–5734.

[31] Pal, R. Phase Modulation Nanoscopy: A Simple Approach to Enhanced Optical Resolution. *Faraday Discuss.* **2015**, *177*, 507–515

ToC Graphic